APPLICATION AND VALIDATION OF REGISTRATION FRAMEWORK FOR REAL-TIME ATLAS GUIDED BIOPSY

[1]*R. Narayanan,* [2]*D. Shen,* [2]*C. Davatzikos,* [3]*D. E. Crawford,* [3]*A. Barqawi,*
[3]*P. N. Werahera,*[1]*D. Kumar, and* [1]*J. S. Suri*

[1]Eigen LLC, 13366 Grass Valley Ave., Grass Valley, CA, USA
[2]Section of Biomedical Image Analysis, Department of Radiology, Univ. of Pennsylvania, PA, USA
[3]University of Colorado at Health Sciences Center, CO, USA

ABSTRACT

It is widely established that prostate cancer is a multifocal disease and cancerous lesions are not uniformly distributed within the gland. Current imaging methods cannot detect prostate cancer with sufficient sensitivity and specificity, especially localized cancers. A cancer atlas was previously demonstrated. However the atlas must be registered with a patient's ultrasound image in a clinical procedure. Here we present the fast registration of this atlas in a clinical setting so as to map cancer likelihoods in addition to optimized biopsy locations from the atlas space to the subject to maximize cancer detection accuracy.

The registration was validated on 158 subjects with cancers annotated and the detection rate was found to be 84.81% and 89.87% for optimized 7 and 12 core biopsy schemes respectively. It took less than 8 seconds for the entire registration procedure.

Index Terms— prostate, cancer, biopsy, registration, atlas

1. INTRODUCTION

The Center for Prostate Disease Research (CPDR) estimates that prostate cancer accounts for nearly 30% of cancers affecting males in the United States in 2007 [1]. Early diagnosis, however shows that the five year survival rate approaches 100%. Prostate specific antigen (PSA) measured via a blood test and the digital rectal examination (DRE) are the most common methods to screen for prostate cancer. Currently localized prostate cancer is diagnosed by tissue confirmation following transrectal ultrasound (TRUS) guided biopsy procedures.

Commonly used TRUS images do not help identify prostate cancers since isoechoic areas and large variabilities in sonographic appearances hardly correlate to cancer.While newer methods such as pulse inversion, color and power Doppler, elastography, contrast and harmonic imaging are starting to gain ground, it is still unclear whether suspicious regions of enhanced TRUS images correlate with localized prostate cancers. A study comparing digital rectal examination (DRE), TRUS-guided biopsy and magnetic resonance (MR) imaging in the detection and localization of prostate cancer showed that MR imaging provided increased accuracy of cancer localization compared to the other two [2]. MR imaging guided transrectal biopsy is feasible but still under investigation. One method that can significantly improve early detection is the use of priors that help direct needles to specific locations that have a statistically high likelihood of developing cancer.

Spatial preference in selecting target locations is further motivated by the work of Naughton *et al*. [3] that demonstrated increasing the number of biopsy cores from 6 to 12 did not yield any improvement, and others (E.g. [4], [5]) that have discussed biopsy protocols sampling regions with higher likelihoods of developing cancer. In a more recent development, the authors in [6] constructed a statistical atlas of prostate cancers that provided voxelwise probabilities of cancer locations. They also devised an optimal sampling scheme for biopsy in the atlas space to maximize cancer detection rates for a given number of biopsy cores. The needle configuration via this approach samples regions that are not statistically correlated with each other maximizing detection likelihood. Ultimately, optimized biopsy schemes that target clinically significant cancers, instead of cancers in general can be constructed using the same approach.

One difficulty in registering the atlas to subjects is the limited availability of time while performing biopsy. Long registration times can increase patient anxiety and risk of motion. Another issue is the accurate registration of the 3D atlas to the subject. Our contribution in this paper is the implementation and validation of the registration method that provides increased cancer detection rates, and the efficient implementation on a graphical processing unit (GPU) to realize speeds less than 8 seconds. In this paper we propose to use a statistical shape model for the registration of the atlas surface with the segmented surface of the subject followed by elastically warping the 3D atlas volume to the subject space. The registration framework was validated by registering the atlas to

histological images whose cancer information is fully known.

2. METHOD

The cancer atlas is a 3D image consisting of cancer probabilities at every voxel. The objective is to register this 3D image to the patient's acquired TRUS image during a biopsy procedure. This involves translation of biopsy locations optimized in the atlas space to the subject, as well as to display a color overlay of cancer probabilities on the TRUS image to help guide target selection during biopsy. The atlas used here was previously developed by our collaborators in [7, 6]. Briefly the registration consists of the following two steps (See fig. 1)

- Step 1: Statistical shape based surface registration of atlas-subject surface
- Step 2: Elastic warping of the atlas volume

In Step 1, a shape model of the prostate is constructed as outlined in [8] from a set of expert segmented prostates (38 in all) to identify the main modes of shape variation. We note that these prostates were derived from ultrasound images of patients, and not from prostatectomy specimens, so that they represent shape variability of the prostate in vivo. Only projections corresponding to these modes and the rotation, scale and translation parameters are optimized so as to maximize similarity of the atlas surface with the subject's surface. The subject's surface at this stage has already been segmented from the acquired TRUS image via a semi-automatic strategy described in [9] taking less than 6 seconds. The model compliant deformation of the atlas is thus estimated as $(\hat{\alpha}, \hat{\mathbf{t}}, \hat{R}, \hat{c}) = \arg\min_{(\alpha,\mathbf{t},R,c)} \|cR(H\alpha + \bar{\mathbf{x}}_\mathbf{s}) + \mathbf{t} - \mathbf{y}\|$, where α is the projection vector on the surface basis of Eigenvectors $H = [\mathbf{v}_1 \mathbf{v}_2 \dots \mathbf{v}_N]$, $\mathbf{t}$, R and c are the global translation, rotation and scale parameters respectively, $\bar{\mathbf{x}}_\mathbf{s}$ is the atlas surface and $\mathbf{y}$ is the segmented subject surface. The surface correspondences estimated from Step 1 are then used to elastically warp the 3D atlas volume in Step 2 using $\mu\boldsymbol{\Delta}\mathbf{u}(\mathbf{x}) + (\mu + \lambda)\nabla(\nabla.\mathbf{u}(\mathbf{x})) + \mathbf{f}(\mathbf{x}) = 0$, where $\mathbf{f}$ is the force field used to drive the flow based on the boundary correspondences.

3. IMPLEMENTATION

The cost function for the shape based registration and elastic warping was implemented using compute unified device architecture (CUDA) on the GPU which is a general purpose application programming interface (API) developed by nVidia, and is highly suited to data parallel computing. The data is split into several hundreds or thousands of threads and implemented in groups of thread blocks on each multiprocessor. Further, access is also provided to a fast parallel cache, called shared memory that allows data cooperation between threads. Data can be temporarily moved here and used for computing

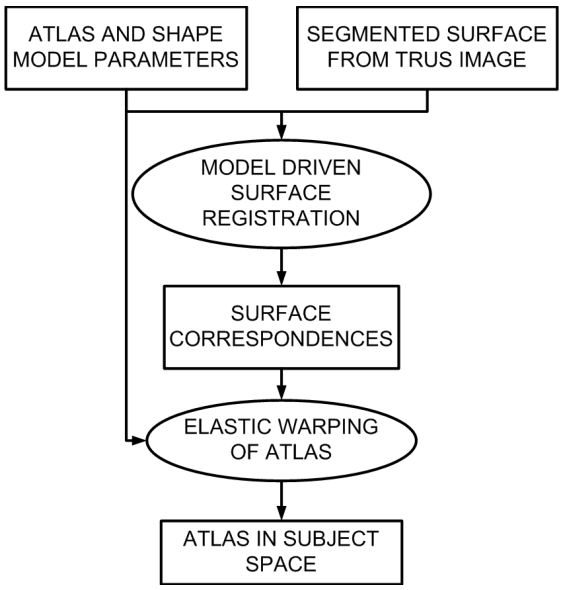

Fig. 1. Atlas Guided Targeted Biopsy

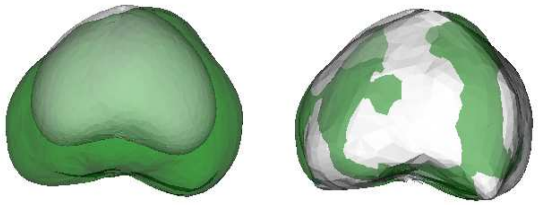

(a) Before Registration (b) After Registration

Fig. 2. Surface Registration in Step 1. The white surface represents the atlas and green represents the subject.

to speed up memory access. Also available are the read-only constant and texture memory.

The Step 1 described in the previous section aims at optimizing the projections on the Eigenvectors to maximize similarity between the atlas surface and the segmented subject. The atlas surface was placed in shared memory, and the subject in constant memory due to the limited space available in shared memory. The registration yielded boundary correspondences on the 3D field and smoothed by the flow $\mathbf{f}$. The elastic warping was implemented by splitting the $64 \times 64 \times 64$ image into sub-blocks ($8 \times 8 \times 8$), where every voxel in the sub-block represented a thread. The threads in this block staged a $10 \times 10 \times 10$ block of data into shared memory, and each thread computed the iterative warps in x, y and z via parallel jacobi relaxation. All data parallel threads were synchronized after each iteration of 500 iterations in total. The key to achieving maximum speed up was found to be via optimal usage of the

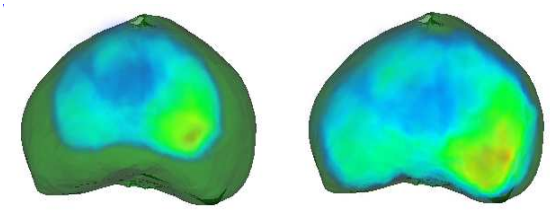

(a) Before Elastic Warping (b) After Warping

Fig. 3. Shows the atlas overlaid on the subject before and after registration

16k shared memory. The registration (steps 1 and 2) took 7.2 seconds to finish offering a significant speed up over the optimized CPU implementation ($\approx$ 30 seconds). Fig. 2a shows the atlas surface and the subject surface overlaid before registration, and Fig. 2b shows the warped atlas surface after registration, and the subject surface. Fig. 3a shows the 3D atlas and the subject surface overlaid before elastic warping while Fig. 3b shows the result of warping the atlas to register with the subject.

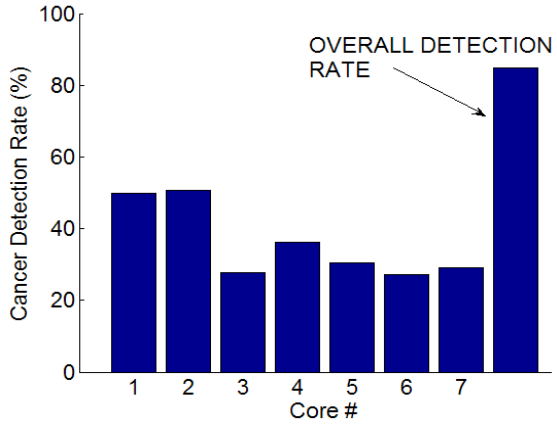

7-Core Detection Rate

Fig. 4. Shows the percentage detection rate for each needle. The last bar shows the overall detection rate

4. RESULTS

Both shape based surface registration and elastic warping ran in 7.2 seconds on an 8800 GTS GPU with 12 multiprocessors and 640 mb memory installed on an Intel Core 2 Duo system with 2 Gb system memory. The elastic warping step took 4.2 seconds for 500 iterations on a $64 \times 64 \times 64$ size 3D atlas.

Since cancers are difficult to detect and annotate on TRUS images, 158, 3D reconstructed histology data from radical

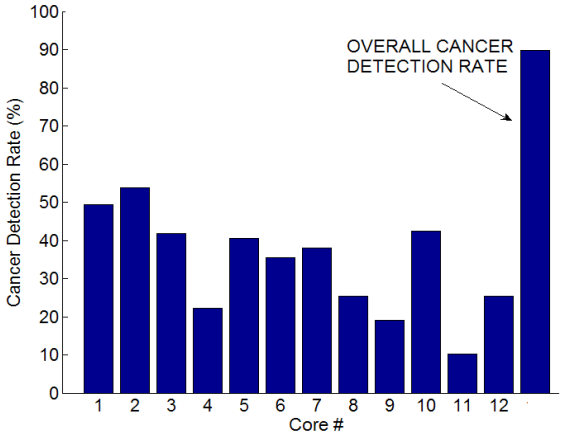

12-Core Detection Rate

Fig. 5. Shows the percentage detection rate for each needle. The last bar shows the overall detection rate

prostatectomy specimen with expert annotated cancers were used as the ground truth. The atlas was registered to each of these images and the detection rate for 7 and 12 core biopsy was estimated. Cancer was considered detected if even one of the cores mapped to a region with cancer. Figures 4 and 5 show the individual detection rate for each biopsy core, and the overall detection rate (last bar in the graph) across all 158 images in the respective protocols. We found the overall detection rate for both protocols to be very high (84.81% and 89.87% for 7 and 12 core biopsy).

5. CONCLUSION

Since the relaxation in Step 2 is highly amenable to parallelization, further improvement in speed may be achieved by running this on a compatible GPU with more multiprocessors and/or more shared memory. The high detection accuracy and fast implementation shows that this system could help improve urologist's workflow significantly in performing biopsy procedures. Future work would involve investigation of detection accuracy of other commonly used biopsy protocols (e.g. sextant, extended 12 core systematic biopsy) defined on the atlas space, and compare with that of 7 and 12 core optimized biopsy presented here.

6. REFERENCES

[1] A Jemal, R Siegel, E Ward, T Murray, J Xu, and M J Thun, "Cancer statistics 2007," *CA Cancer J Clin*, 2007.

[2] M Mullerad, H Hricak, K Kuroiwa, D Pucar, H Chen, M Kattan, and P Scardino, "Comparison of endorectal magnetic resonance imaging, guided prostate biopsy and digital rectal examination in the preoperative anatomical

localization of prostate cancer," *The Journal of Urology*, vol. 174, pp. 2158–2163.

[3] C K Naughton, D C Miller, D E Mager, D K Ornstein, and W J Catalona, "A prospective randomized trial comparing 6 versus 12 prostate biopsy cores: impact on cancer detection," *J Urol.*, vol. 164, pp. 388–392.

[4] M E Chen, P Troncoso, K Tang, R J Babaian, and D Johnston, "Comparison of prostate biopsy schemes by computer simulation," *J Urol.*, vol. 53, pp. 951–960.

[5] M B Opell, J Zeng, J J Bauer, R R Connelly, W Zhang, I A Sesterhenn, S K Mun, J W Moul, and J H Lynch, "Investigating the distribution of prostate cancer using three-dimensional computer simulation," *Prostate Cancer and Prostatic Diseases*, vol. 5, pp. 204–208, 2002.

[6] Y Zhan, D Shen, J Zeng, L Sun, G Fichtinger, J Moul, and C Davatzikos, "Targeted prostate biopsy using statistical image analysis," *IEEE Trans. Med. Imag.*, vol. 26, no. 6, pp. 779–788, 2007.

[7] D Shen, Z Lao, J Zeng, W Zhang, I A Sesterhenn, L Sun, J W Moul, E H Herskovits, G Fichtinger, and C Davatzikos, "Optimized prostate biopsy via a statistical atlas of cancer spatial distribution," *Medical Image Analysis*, vol. 8, pp. 139–150, 2004.

[8] T F Cootes, C J Taylor, D H Cooper, and J Graham, "Active shape models - their training and application," *Computer Vision and Image Understanding*, vol. 61, no. 1, pp. 38–59, 1995.

[9] H M Ladak, F Mao, Y Wang, D B Downey, D A Steinman, and A Fenster, "Prostate boundary segmentation from 2d ultrasound images," *Engg. in Medicine and Biology Society, Proc of the 22nd Annual Int. Conf. of IEEE*, vol. 4, pp. 3188–3191, 2000.